Buoyancy Induced Heat Transfer in a Trapezoidal Enclosure with Offset Baffles

F. Moukalled* and M. Darwish
Department of Mechanical Engineering
American University of Beirut
P.O.Box 11-0236
Riad El Solh, Beirut 1107 2020
Lebanon

ABSTRACT

A numerical study has been conducted to examine the effects on heat transfer of mounting two offset baffles onto the upper inclined and lower horizontal surfaces of trapezoidal cavities. Two thermal boundary conditions are considered. In the first, the left short vertical wall is heated while the right long vertical wall is cooled (buoyancy assisting mode along the upper inclined surface of the cavity). In the second, the right long vertical wall is heated while the left short vertical wall is cooled (buoyancy opposing mode along the upper inclined surface of the cavity). For both boundary conditions, computations are performed for: several offset baffle heights, four Rayleigh number values, three Prandtl (Pr) number values, and two baffle positions (Position I and Position II). In Position I, the lower baffle is offset toward the short vertical wall and the upper baffle is offset toward the long vertical wall of the enclosure, whereas in Position II, the lower and upper baffles are offset toward the long and short vertical walls, respectively. Results reveal a decrease in heat transfer in the presence of baffles with its rate generally increasing with increased baffle height and Pr. At a given baffle height and Ra, Nu values are lower in the buoyancy opposing mode. For both boundary conditions, the highest decrease is achieved in fully partitioned enclosures.

^{*} Author to whom all correspondence should be addressed. Email: memouk@aub.edu.lb

NOMENCLATURE

A area

c_P specific heat of fluid

g gravitational acceleration

H height of the short vertical wall

H* height of the cavity at the location of the baffle

H_b height of baffle

i unit vector in x-direction

j unit vector in y-direction

k thermal conductivity

k_b baffle thermal conductivity

 k_r conductivity ratio (k_b/k)

L enclosure width

L_b distance between short wall and baffle

n normal unit vector at baffle-air interface

Nu local Nusselt number

Nu average Nusselt number

p,P dimensionless and dimensional pressure

Pr Prandtl number $(=\mu c_P/k)$

Q heat flux

Ra Rayleigh number $(=g\beta(T_h - T_c)H^3/\nu\alpha)$

- T dimensional temperature
- u, U dimensionless and dimensional horizontal velocity component
- **u** dimensionless velocity vector
- v, V dimensionless and dimensional vertical velocity component
- W_b baffle thickness
- x, X dimensionless and dimensional coordinate along the horizontal direction
- y, Y dimensionless and dimensional coordinate along the vertical direction

GREEK SYMBOLS

- β coefficient of thermal expansion
- μ viscosity
- v kinematic viscosity (μ/ρ)
- θ dimensionless temperature
- ρ density

SUBSCRIPTS

- b baffle
- c cold wall
- h hot wall
- i condition at baffle-air interface
- l lower
- max maximum value
- u upper

INTRODUCTION

Buoyancy induced heat transfer in enclosures is still attracting the attention of many researchers due to its relevance to many engineering applications involving among others cooling of electronic equipment, solar collectors, solidification, nuclear waste disposal, and natural convection in attics. The hydrodynamics and heat transfer characteristics being highly dependent on the geometry and boundary conditions of the enclosure result in fundamental solutions specific to the configuration at hand and necessitate obtaining new solutions for new configurations. This article reports on a numerical investigation conducted to explore the effects of attaching two offset baffles to the lower horizontal base and upper inclined surface of a trapezoidal enclosure.

Extensive work on natural convection heat transfer in regular shaped enclosures was reported in the literature, a review of which can be found in [1,2]. However in many practical problems the buoyancy-induced flows are usually surrounded by complicated-shaped boundaries. Since it is difficult to envisage solutions a priori from those obtained in regular enclosures, attention has recently been directed towards studying buoyancy-induced heat transfer in enclosures of irregular shapes.

Experimental and theoretical investigations of natural convection heat transfer in an inclined trapezoidal cavity formed from parallel cylindrical top and bottom walls and adiabatic side walls were reported by Iyican et al. [3,4]. Similarly, Lam et al. [5] reported experimental and numerical natural convection results in a trapezoidal cavity formed from two vertical adiabatic side walls, a horizontal hot bottom wall, and an inclined cold top wall. Experimental measurements revealed that the two-dimensional numerical model

used in [5] is capable of predicting heat transfer rates to an acceptable level of accuracy. Numerical results for laminar natural convection in trapezoidal enclosures with insulated horizontal bottom and top walls and inclined hot and cold sidewalls were reported by several researchers [6-10]. The Lee [6,7] and Peric [8] predictions were limited to a Rayleigh number value of 10⁵, the Sadat and Salagnac [9] results were for Rayleigh number values ranging from 10³ to 2x10⁵, and the Kuyper and Hoogendoorn [10] computations were for Rayleigh numbers between 10⁴ and 10⁸. Transient results in the enclosure were recorded by Karyakin [11]. Ridouane et al. [12] reported on natural convection heat transfer in an attic space with sloped roofs and horizontally suspended ceilings for summer-like and winter-like boundary conditions. Depending on the slope of the roof, the shape varied from an isosceles triangular enclosure to a trapezoidal enclosure. Their study revealed that the presence of insulated side walls provides a sizable saving in energy to keep the attic at the desired temperature during both summer and winter.

Studies on buoyancy-induced heat transfer in partially divided trapezoidal cavities are limited to the ones reported by Moukalled and Acharya [13-15], and Moukalled and Darwish [15,16]. Moukalled and Acharya [13-15] investigated numerically, for summer-like and winter-like boundary conditions, the effect on natural convection heat transfer of partially dividing a trapezoidal enclosure. In [13,14] the partial dividers were attached to the lower horizontal base [13] and upper inclined surface [14] of the cavity. In [15] however, two offset partial vertical dividers attached to the upper inclined surface and the lower horizontal base of the cavity, were employed. The studies reported by Moukalled and Darwish [16,17] differ from the previous ones in the geometry and boundary

conditions. The enclosure used in this work, similar to that employed in [16,17], is half the one studied in [13-15] and the left vertical boundary is a wall boundary (symmetry boundary in [13-15]). However unlike the configurations in [16,17] where a baffle was either attached to the lower horizontal base [16] or the upper inclined surface of the cavity [17], two offset partial dividers attached to the lower and upper surfaces are used.

PHYSICAL MODEL AND GOVERNING EQUATIONS

Figure 1a is a schematic of the enclosure examined in this study. The baffles protrude from the lower horizontal base and upper inclined surface of the trapezoidal cavity. Their finite width, W_b , is fixed at 5% of the enclosure width, L, in all computations. Their heights, $H_{b,l}$ and $H_{b,u}$, are independently assigned four different values $(0, H^*/3, 2H^*/3, and H^*, where H^*$ is the height of the cavity at the location of baffle). In addition, two offset baffle positions $(L_{b,l}=L/3, L_{b,u}=2L/3 \text{ (Position I)}$ and $L_{b,l}=2L/3, L_{b,u}=L/3 \text{ (Position II)}$ are considered. As shown in Figure 1a, $L_{b,l}$ $(L_{b,u})$ represents the distance from the short vertical wall to the lower (upper) baffle. Moreover, the height of the short vertical wall of the cavity, H, is $\frac{1}{4}$ the width, L (H=L/4). With the inclination of upper surface fixed at 15° , the height of the tall vertical wall is $\approx 2.072H$.

The effects of the presence of the partial dividers on the hydrodynamics and heat transfer characteristics in the cavity are analyzed under buoyancy-aiding and buoyancy-opposing boundary conditions. For both conditions, the lower horizontal base and upper inclined plane of the cavity are insulated. The difference is in the conditions maintained on the vertical walls. For the buoyancy-aiding mode, the left short vertical wall of the cavity is maintained at the uniform hot temperature T_h and the right long vertical wall is

maintained at the uniform cold temperature T_c . For the buoyancy opposing mode, the left wall is cold (T_c) while the temperature of the right wall is T_h .

The equations governing the flow and heat transfer are those expressing the conservation of mass, momentum, and energy. The flow is assumed to be laminar, steady, and two-dimensional with constant fluid properties, except for the induced variations in the body force term. The transport equations are non-dimensionalized using the following dimensionless variables:

$$x = \frac{X}{H}, y = \frac{Y}{H}, u = \frac{U}{v/H}, v = \frac{V}{v/H}, p = \frac{P + \rho gy}{\rho(v/H)^2}, \theta = \frac{T - T_c}{T_b - T_c}$$
 (1)

With the stated assumptions and the Boussinesq approximation, the dimensionless governing transport equations of mass, momentum, and energy are, respectively, written as

$$\nabla \cdot \mathbf{u} = 0 \tag{2}$$

$$\mathbf{u} \cdot \nabla \mathbf{u} = -\mathbf{i} \cdot \nabla \mathbf{p} + \nabla \cdot \nabla \mathbf{u} \tag{3}$$

$$\mathbf{u} \cdot \nabla \mathbf{v} = -\mathbf{j} \cdot \nabla \mathbf{p} + \nabla \cdot \nabla \mathbf{v} + \frac{\mathbf{Ra}}{\mathbf{Pr}} \mathbf{\theta} \tag{4}$$

$$\mathbf{u} \cdot \nabla \theta = \frac{1}{\Pr} \nabla \cdot \nabla \theta \tag{5}$$

In the baffle region, the only conservation equation needed is the Laplace equation and is given by

$$\frac{\mathbf{k_b}/\mathbf{k}}{\mathbf{Pr}} \left(\nabla \cdot \nabla \theta_{\mathbf{b}} \right) = 0 \tag{6}$$

where k_b and θ_b denote the thermal conductivity and non-dimensional temperature in the baffle, respectively. The energy balance at the baffle-air interface can be stated as

$$-\frac{1}{\mathbf{Pr}} [(\nabla \theta) \cdot \mathbf{n}]_{i} = -\frac{\mathbf{k}_{b} / \mathbf{k}}{\mathbf{Pr}} [(\nabla \theta_{b}) \cdot \mathbf{n}]_{i}$$
(7)

where \mathbf{n} is a unit vector in the direction normal to the baffle-air interface and the subscript i refers to the interface.

The hydrodynamic and thermal boundary conditions needed to solve the above system of equations (Eqs. (2)-(5)) are the no-slip condition on the enclosure walls, non-dimensional uniform temperatures of 1 and 0 along the hot and cold walls, and the zero temperature gradient along the insulated walls.

After calculating the velocity and temperature fields, the local and average Nusselt numbers along the hot or cold vertical wall are calculated as

$$Nu = h\ell/k \qquad \overline{Nu} = \frac{1}{\ell} \int_{0}^{\ell} NudX$$
 (8)

where ℓ is the height of the hot or cold wall. Based on this definition, the average Nusselt number values along both walls are equal. Moreover, the heat transfer coefficient h is defined as

$$\dot{Q} = hA(T_h - T_c) = -kA\frac{dT}{dX}$$
(9)

Using dimensionless quantities, the following relation for the heat transfer coefficient is obtained:

$$h = -\frac{k}{H} \frac{d\theta}{dx} \tag{10}$$

SOLUTION PROCEDURE

A collocated Finite Volume Method (FVM) is used to solve the coupled system of equations governing the flow and temperature fields (Eqs. (2)-(5)). Checkerboard

pressure and velocity fields are eliminated through the use of the Momentum Weighted Interpolation Method (MWIM) for the calculation of the mass fluxes across the control volume faces [18]. Pressure-velocity coupling is accomplished through the use of the SIMPLE algorithm of Patankar [19]. Solutions are obtained by subdividing the physical space into a number of control volumes with grid points placed at their geometric centers (Figure 1b). The discretized equations are obtained through a two-step procedure. In step 1, the conservation equations are integrated over a control volume (Figure 1a) to obtain a discretized description of the conservation law. In step 2, an interpolation profile is used to reduce the integrated equations to algebraic equations by expressing the variation in the dependent variable and its derivatives in terms of the grid point values. The approximation scheme produces an expression for the face value which is dependent on the nodal values in the vicinity of the face. The diffusion flux is discretized along each surface of the control volume using the method described in Zwart et al. [20], while the convective flux is calculated using the third order SMART scheme [21] applied within the context of the NVSF methodology [22]. In addition, the integral value of the source term over the control volume P (Figure 1b) is evaluated by assuming the estimate of the source at the control volume center to represent the mean value over the whole control volume. Then, the set of algebraic equations is solved iteratively using the Tri-Diagonal Matrix Algorithm (TDMA) [19]. Moreover, the grid (Figure 1c) is generated using the transfinite interpolation technique [23]. Furthermore, the presence of the baffle in the calculation domain is accounted for by the special treatment suggested by Patankar [19]. Finally, since a conservative scheme is used, arranging the control volume face to coincide with the divider interface ensures energy balance at the baffle-air interface and forces equation (7) to be implicitly satisfied.

NUMERICAL ACCURACY

Grid-independent solutions were established by comparing solutions generated on different grid sizes. A final non-uniform mesh of size 122x122 grid points was used in generating all results presented in this paper. The grid points were concentrated close to solid boundaries where large gradients are expected (Figure 1c). The accuracy of the calculations was verified by comparing representative computed profiles of velocity, temperature, and local Nusselt number values using the 122x122 non-uniform grid with those obtained on a 240x240 nearly uniform grid. The maximum difference between the two solutions in the various quantities predicted was smaller than 0.1%. Conservation of the various physical quantities was satisfied to within 10⁻⁵ % in each control volume.

RESULTS AND DISCUSSION

The governing parameters in the problem are the Prandtl number (Pr), the Rayleigh number (Ra), the conductivity ratio (k_r), the heights of the upper and lower baffles ($H_{b,l}$ and $H_{b,u}$), and the relative position of the offset baffles. For both boundary conditions, results are obtained for four baffle heights (0, $H^*/3$, $2H^*/3$, and H^*), two offset baffle configurations ($L_{b,l}=L/3$, $L_{b,u}=2L/3$ (Position I) and $L_{b,l}=2L/3$, $L_{b,u}=L/3$ (Position II)), three Prandtl numbers (Pr=0.7, 10, and 130), and Rayleigh number values varying between 10^3 and 10^6 . Moreover, the conductivity ratio is fixed at 2 to simulate a poorly

conducting divider. Results are presented in the form of representative streamlines, isotherms, and local and average Nusselt number values.

BUOYANCY-AIDING MODE

Streamlines and isotherms

Representative streamline and isotherm plots for Pr=0.7 are displayed in Figures 2-4. For Position I, the flow patterns and temperature distributions are depicted in Figure 2 for the case where the lower and upper baffles are at heights $H_{b,u}=2H_u^*/3$ and $H_{b,l}=2H_l^*/3$, respectively. Results indicate that at low and moderate Ra values (Figures 2a and 2b) the flow consists of three counterclockwise rotating vortices communicating through a thin overall rotating eddy. The clockwise rotation of the flow indicates that it moves up along the left hot vertical and insulated inclined walls, then turns around the upper baffle, down along the cold wall, and then to the left along the horizontal base of the cavity and around the lower baffle.

As Ra increases to 10⁵ (Figure 2c), the fluid rising along the left hot vertical wall becomes more buoyant allowing deeper penetration into the right portion of the domain, the interaction between the vortices increases, the eyes of the circulating eddies elongate, and the middle core disintegrates in favor of the right and left vortices. With further increase in Ra to 10⁶ (Figure 2d), clearer separation of the vortices occur with formation of two jet-like flows. The first one, which is directed from the hot wall to the left baffle tip, impinges on the left face of the upper baffle and returns back to the left portion of the cavity. The second jet-like flow, which is directed from the cold wall to the right baffle tip, impinges on the right face of the baffle attached to the lower horizontal base of the

cavity and returns back to the right portion of the cavity. This behavior is due to the increase of the stratification level in the enclosure with increasing Ra value as clearly seen by the isotherms presented in Figures 2e-2h. At low Ra (Ra=10³, Figure 2e), isotherms are uniformly distributed between the hot and cold walls showing dominant conduction heat transfer. As Ra values increase, the distribution of isotherms implies higher stratification levels within the enclosure (compare Figures 2e-2h) and consequently higher convection contribution. In addition, the boundary-layer-type flow along the hot and cold walls becomes clearer.

For Position II, streamline and isotherm maps are displayed in Figure 3. As depicted, for Ra= 10³ and 10⁴ the hydrodynamic (Figures 3a and 3b) and thermodynamic (Figures 3e and 3f) features of the flow are similar to those presented in Figures 2a and 2b (Position I) with the flow field being composed of three vortex cores rotating in a clockwise direction. As Ra increases (Figures 3c and 3d), communication between the inner vortices increases and streamlines reveal that increasing amounts of the flow, moving down the right cold vertical wall, is deflected off it near the lower baffle tip. This is due to thermal stratification (Figures 3g and 3h) in the lower right portion of the domain between the divider and the cold wall, which inhibits flow penetration into these regions.

Representative streamlines and isotherms showing the effects of baffle height on the velocity and temperature fields are presented in Figure 4 in an enclosure with offset baffles (Position I) of heights 0, H*/3, 2H*/3, and H* for a Ra of 10⁵.

The maximum strength of the flow is in the baffle-free enclosure (Figure 4a), which is composed of a single vortex rotating clockwise. As the offset baffle height increases, a weaker flow is observed in the cavity. For a fully partitioned enclosure (Figure 4d), three

similar clockwise rotating eddies are apparent with their strength lower than the single vortex flow in the non-partitioned cavity. This is due to smaller convective area in each part combined with a decrease in the available temperature difference. These findings are reflected on the maps presented in Figures 4e-4h, which clearly show the decrease in convection heat transfer through the spread of isotherms.

Nusselt numbers

Typical local Nusselt number variations (Nu) along the hot and cold vertical walls are presented in Figure 5. Values are plotted as a function of Y/Y_{max} where Y_{max} is the height of the hot or cold vertical wall. The effect of Ra on Nusselt number values is displayed along the hot and cold walls in Figures 5a and 5b, respectively, for an enclosure with baffle heights of $H_{b,u} = 2H_u^*/3$ and $H_{b,l} = 2H_l^*/3$ placed in Position I. The local value of the Nusselt number decreases as the fluid moves upward along the hot wall and downward along the cold wall due to a decrease in the temperature difference between the fluid and the wall. As depicted, the Nusselt number levels increase with increasing values of Ra indicating higher convection contribution to the total heat transfer. Moreover, Nu peaks at the upper section of the cold wall at the location of impingement of the hot rising fluid. Similar peaks occur in both the lower and upper parts of the hot wall but are not as sharp. The steepness of the peak as the hot fluid impinges on the cold wall is due to the aiding effects of buoyancy along the upper inclined plane of the enclosure, which further increases the velocity of the hot fluid before striking the cold wall. The Nusselt number distributions along the hot and cold walls, displayed respectively in Figures 5c and 5d, in an enclosure with offset baffles in Position I at a Ra value of 10⁵ clearly reveal the decrease in heat transfer as the offset baffle heights increase. This decrease is due to a reduction in the convection contribution to total heat transfer caused by the presence of the partial dividers, which interrupt the convective motion and reduce the convection heat transfer coefficient.

The average Nusselt number $(\overline{\text{Nu}})$ values in the enclosure are presented in Table 1. In comparison with a baffle free enclosure, the presence of the baffles generally reduces the amount of heat transported across the cavity with the percentage of reduction increasing with increasing baffles heights and Rayleigh number values. Moreover, the heat transfer is normally lower for a cavity with offset baffles in Position I. This is due to the fact that in Position I the upper baffle is located closer to the cold wall than in Position II, which interrupts the convective motion at a distance closer to the cold wall before impinging it. As expected, $\overline{\text{Nu}}$ increases with increasing Pr due to a decrease in the thermal boundary layer thickness along the walls with a consequent increase in the temperature gradient. The rate of increase slows down as the Prandtl number increases with the values for Pr=10 and Pr=130 being very close.

BUOYANCY-OPPOSING MODE

Streamlines and isotherms

For the buoyancy-opposing heat transfer mode, streamlines and isotherms are presented in Figures 6-8 with a value of Pr=0.7, representing air as the working fluid. Figures 6 and 7 reveal the effects of Ra on the flow and the heat transfer characteristics for a partitioned enclosure with offset baffles of heights $H_{b,u} = 2H_u^*/3$ and $H_{b,l} = 2H_l^*/3$ placed in positions I and II, respectively. Opposite to the buoyancy-aiding situation (Figure 2), the fluid in the enclosure moves in a counterclockwise direction. By comparing results in Figures 6

and 7 against results in Figures 2 and 3 it is easy to notice that for the buoyancy-opposing mode the flow structure over a domain with baffles in Position I (Figure 6) are similar to those for the buoyancy-aiding mode with baffles placed in Position II (Figure 3), and vice versa (i.e. similarity of flow structure in Figures 7 and 2). For both baffle positions, the flow characteristics are similar at low Ra values (Figures 6a and b and Figures 7a and b) with the flow field being composed of three recirculation zones. As Ra increases, baffle position becomes important and the flow characteristics change with the middle recirculation zone increasing in size for Position I while splitting and forming a jet-like flow for baffles placed in Position II. In both positions, as Ra increases the eyes of the recirculation zones elongate and move towards the bottom of the domain (opposite to the buoyancy-aiding mode). No separation of the fluid on either side of the dividers was noted. By comparing streamlines in Figure 6 against those reported in Figure 7 it can be inferred that, for $H_{b,u} = 2H_u^*/3$ and $H_{b,l} = 2H_l^*/3$, placing the upper divider close to the hot wall intensifies the middle recirculation zone, which is expected to increase convection heat transfer across the cavity.

At Ra=10³ the temperature uniformly varies over the domain. As Ra increases, isotherms become more distorted revealing an increase in convection contribution to heat transfer in the cavity. Moreover, at high Ra values (Figures 6g, 6h, 7g, and 7h) isotherms reveal high stratification levels on the top right side of the domain where the rising hot fluid has to descend along the inclined top surface of the enclosure.

Figure 8 reveals the effects of baffle height in an enclosure with offset baffles in Position I and for Ra=10⁵. In the absence of baffles (Figure 8a), the flow in the enclosure is composed of a single counterclockwise rotating cell. At this value of Ra, the eye of the

recirculation is elongated and is about to separate into two smaller vortices one close to the hot wall and the other close to the cold wall. As the height of baffles increases, the flow becomes weaker (Figures 8a-8d) and a decrease in convection effects is observed which is manifested by a lighter clustering of isotherms along the hot and cold walls (Figures 8e-8h).

Nusselt numbers

Representative plots showing the distribution of Nusselt number values along the vertical walls of the enclosure are displayed in Figure 9. The effects of Ra on heat transfer are depicted in Figures 9a and 9b where variations in local Nu estimates are displayed along the cold and hot walls of a cavity with offset baffles of heights $H_{b,u} = 2H_u^*/3$ and $H_{b,l} = 2H_l^*/3$ placed in Position I. It is easily inferred from the figures that convection heat transfer increases with increasing values of Ra. Along both the cold (Figure 9a) and hot (Figure 9b) walls, the Nusselt number decreases in the direction of fluid motion and results in the variations shown by the figures. This decrease is due to the decrease in the temperature difference between the fluid and the wall (the fluid cools along the cold wall and heats along the hot wall). Moreover, the high Nu value near $Y/Y_{max}=1$ (Figure 9a), is due to the large temperature difference between the hot fluid and the cold wall. Furthermore, the peak at the leading edge in Figure 9b is caused by the impingement of the cold fluid on the hot wall while trying to negotiate the corner. The effect of baffle height on heat transfer is presented in Figures 9c and 9d for Ra=10⁵. When baffle heights are increased, plots reveal a decrease in Nu values along the hot and cold walls as a consequence of the decrease in convection heat transfer.

The average Nusselt number (\overline{Nu}) values for all cases studied are displayed in Table 2. As expected, values are lower than their counterparts displayed in Table 1 for the buoyancy-aiding mode. The average Nusselt number increases with increasing Ra values. Further, Nu in a partitioned cavity is lower than its value in a baffle free cavity indicating a reduction in convection heat transfer due to the presence of baffles. At Ra=10³, there exists a baffle height at which the decrease in heat transfer is maximized. This optimum height is dictated by the competing effects of convection and diffusion which decrease and increase, respectively, with the increase in either of the offset baffle heights. At Ra $\geq 10^4$, convection is the dominant heat transfer mode and $\overline{\text{Nu}}$ decreases with increasing offset baffle heights with the lowest value obtained for the fully partitioned cavity (i.e. when $H_{b,u} = H_u^*$ and $H_{b,l} = H_l^*$). In both baffle positions, the lower baffle is more effective in reducing heat transfer than the upper baffle with this effectiveness being higher for offset baffles in Position I (e.g. at Ra= 10^6 , $\overline{\text{Nu}} = 6.145$ for $H_{b,u} = 2H_u^*/3$ and $H_{b,l} = H_l^*/3$ while $\overline{Nu} = 4.021$ for $H_{b,u} = H_u^*/3$ and $H_{b,l} = 2H_l^*/3$). As in the buoyancy-assisting case, \overline{Nu} increases with increasing Pr due to an increase in the temperature gradient along the walls. Again, the rate of increase goes down as the Prandtl number increases with the values for Pr=10 and Pr=130 being almost identical.

CLOSING REMARKS

Natural convection in a trapezoidal enclosure with offset baffles mounted onto its upper inclined and lower horizontal surface has been studied numerically. For the two offset baffle positions considered (Positions I and II), the effects of the Rayleigh number,

Prandtl number, and baffle height on heat transfer were investigated. Two boundary conditions were studied representing buoyancy assisting and buoyancy opposing modes along the upper inclined surface of the cavity. Results revealed a reduction in heat transfer in the presence of baffles with its rate increasing with increasing Pr and/or offset baffle heights. The heat transfer level was found to be lower in the buoyancy opposing case.

ACKNOWLEDGMENTS

The financial support provided by the Lebanese National Council for Scientific Research (LNCSR) through Grant No. 022142 is gratefully acknowledged.

REFERENCES

- Ostrach, S., "Natural Convection in Enclosures," *Journal of Heat Transfer*, vol. 110, pp. 1175-1190, 1988.
- 2. Jaluria, Y., Natural Convection, in A. Bejan and A.D. Kraus (eds.), *Heat Transfer Handbook*, chap. 7, Wiley, New York, 2003.
- 3. Iyican, L., Bayazitoglu, Y., and Witte, L., "An Analytical Study of Natural Convective Heat Transfer within a Trapezoidal Enclosure," *Journal of Heat Transfer*, vol. 102, pp. 640-647, 1980.
- Iyican, L., Witte, L.C., and Bayazitoglu, Y., "An Experimental Study of Natural Convection in Trapezoidal Enclosures", *Journal of Heat Transfer*, vol. 102, pp. 648-653, 1980.
- Lam, S.W., Gani, R., and Simons, J.G., "Experimental and Numerical Studies of Natural Convection in Trapezoidal Cavities," *Journal of Heat Transfer*, vol. 111, pp. 372-377, 1989.
- Lee, T.S., "Numerical Experiments with Fluid Convection in Tilted Nonrectangular Enclosures," *Numerical Heat Transfer*, Part A, vol. 19, pp. 487-499, 1991.
- Lee, T.S., "Computational and Experimental Studies of Convective Fluid Motion and Heat Transfer in Inclined non-rectangular enclosures," *International Journal of Heat* and Fluid Flow, vol.5, pp. 29-36, 1984.
- 8. Peric', M., "Natural Convection in Trapezoidal Cavities," *Numerical Heat Transfer*, Part A, vol. 24, pp. 213-219, 1993.

- Sadat, H. and Salagnac, P., "Further results for Laminar Natural Convection in a Two-dimensional Trapezoidal Enclosure," *Numerical Heat Transfer*, Part A, vol. 27, pp. 451-459, 1995.
- 10. Kuyper, R.A. and Hoogendoorn, C.J., "Laminar Natural Convection Flow in Trapezoidal Enclosures," *Numerical Heat Transfer*, Part A, vol. 28, pp. 55-67, 1995.
- 11. Karyakin, Y.E. "Transient Natural Convection in Prismatic Enclosures of Arbitrary cross-section," *International Journal of Heat and Mass Transfer*, vol. 32, no. 6, pp. 1095-1103, 1989.
- 12. Ridouane, H., Campo, A., and Hasnaoui, M.," Benefits Derivable From Connecting the Bottom and Top Walls of Attic Enclosures with Insulated Vertical Wall," *Numerical Heat Transfer*, Part A, vol. 49, pp. 175-193, 2006.
- 13. Moukalled, F. and Acharya, S., "Buoyancy-Induced Heat Transfer in Partially Divided Trapezoidal Cavities," *Numerical Heat Transfer*, Part A, vol. 32, pp. 787-810, 1997.
- 14. Moukalled, F. and Acharya, S., "Natural Convection in Trapezoidal Cavities with Baffles Mounted on The Upper Inclined Surfaces," *Numerical Heat Transfer*, Part A, vol. 37, no. 6, pp.545-565, 2000.
- 15. Moukalled, F. and Acharya, S., "Natural Convection in a Trapezoidal Enclosure with Offset Baffle," *AIAA Journal of Thermophysics and Heat Transfer*, vol. 15, no. 2, pp. 212-218, 2001.
- 16. Moukalled, F. and Darwish, M., "Natural Convection in a Partitioned Trapezoidal Cavity Heated from the Side," *Numerical Heat Transfer*, Part A, vol. 43, pp. 543-563, 2003.

- 17. Moukalled, F. and Darwish, M., "Natural Convection in a Trapezoidal Enclosure Heated from the Side with a Baffle Mounted on Its Upper Inclined Surface," *Heat Transfer Engineering*, vol. 25, no. 8, pp. 80-93, 2004.
- 18. Peric, M., "A Finite Volume Method for the Prediction of Three Dimensional Fluid Flow in Complex Ducts," Ph.D. Thesis, Imperial College, Mechanical Engineering Department, London, 1985.
- 19. Patankar, S.V., *Numerical Heat Transfer and Fluid Flow*, New York, Hemisphere Publishing Corporation, 1980.
- 20. Zwart, P.J., Raithby, G.D., and Raw, M.J., "An Integrated Space-Time Finite-Volume Method for Moving-Boundary Problems," *Numerical Heat Transfer*, Part B, vol. 34, pp. 257-270, 1998.
- 21. Gaskell, P.H. and Lau, A.K.C., "Curvature Compensated Convective Transport: SMART, A New Boundedness Preserving Transport Algorithm," *International Journal for Numerical Methods in Fluids*, vol. 8, pp. 617-641, 1988.
- 22. Darwish, M. and Moukalled, F., "Normalized Variable and Space Formulation Methodology for High-Resolution Schemes," *Numerical Heat Transfer*, Part B, vol. 26, pp. 79-96, 1994.
- 23. Gordon, W.J. And Theil, L.C., "Transfinite Mappings and Their Applications to Grid Generation," in Thompson J.F. (ed.), *Numerical Grid Generation*, North Holland, New York, pp. 171-192, 1982.

LIST OF TABLES

- Table 1 Average Nusselt number values \overline{Nu} for hot left wall and cold right wall (buoyancy assisting boundary condition).
- Table 2 Average Nusselt number values \overline{Nu} for cold left wall and hot right wall (buoyancy opposing boundary condition).

FIGURE CAPTIONS

- Figure 1 (a) Physical domain; (b) a typical control volume; (c) computational domain and
 - an illustrative grid network.
- Figure 2 Streamline and isotherm plots ($H_{b,u} = 2H_u^*/3$, $H_{b,l} = 2H_l^*/3$, Position I) for the buoyancy assisting boundary condition.
- Figure 3 Streamline and isotherm plots ($H_{b,u} = 2H_u^*/3$, $H_{b,l} = 2H_l^*/3$, Position II) for the buoyancy assisting boundary condition.
- Figure 4 Streamline and isotherm plots (Ra=10⁵, Position I) at different baffles height for the buoyancy assisting boundary condition.
- Figure 5 Local Nusselt number distribution along (a,c) hot walls and (b,d) cold walls for the buoyancy assisting boundary condition, Position I; (a,b) effects of Ra $(H_{b,u} = H_u^*/3, H_{b,l} = H_l^*/3); (c,d) \text{ effects of baffle heights } (Ra=10^5).$
- Figure 6 Streamline and isotherm plots ($H_{b,u} = 2H_u^*/3$, $H_{b,l} = 2H_l^*/3$, Position I) for the buoyancy opposing boundary condition.
- Figure 7 Streamline and isotherm plots ($H_{b,u} = 2H_u^*/3$, $H_{b,l} = 2H_l^*/3$, Position II) for the buoyancy opposing boundary condition.
- Figure 8 Streamline and isotherm plots (Ra=10⁵, Position I) at different baffles height for the buoyancy opposing boundary condition.
- Figure 9 Local Nusselt number distribution along (a,c) hot walls and (b,d) cold walls for the buoyancy assisting boundary condition, Position I; (a,b) effects of Ra $(H_{b,u} = H_u^*/3, H_{b,l} = H_l^*/3); (c,d) \text{ effects of baffle heights } (Ra=10^5).$

Table 1 Average Nusselt number values \overline{Nu} for hot left wall and cold right wall (buoyancy assisting boundary condition).

Position I ($L_{b,l}=L/3$, $L_{b,u}=2L/3$)												
	$H_{b,u}$	$H_u^*/3$	2H _u */3	$\overline{H}^*_{\mathrm{u}}$	$H_u^*/3$	2H _u */3	H_{u}^{*}	$H_u^*/3$	2H _u */3	H_{u}^{*}		
Ra	No Baffle	$H_{b,l} = H_1^*/3$			$H_{b,l} = 2H_1^*/3$			$H_{b,l} = H_l^*$				
Pr=0.7												
10^{3}	0.715	0.462	0.421	0.424	0.438	0.405	0.407	0.443	0.408	0.410		
10^{4}	2.48	1.840	1.141	1.093	1.049	0.786	0.769	1.041	0.783	0.766		
10 ⁵	5.476	4.987	2.943	2.288	2.952	2.091	1.755	2.062	1.664	1.394		
10^{6}	10.925	10.354	5.915	3.930	6.867	4.362	3.468	3.529	3.058	2.312		
Pr=10												
10^{3}	0.719	0.462	0.422	0.424	0.438	0.405	0.407	0.443	0.408	0.410		
10^{4}	2.666	1.873	1.157	1.109	1.065	0.794	0.775	1.055	0.789	0.771		
10^{5}	6.102	5.402	3.074	2.384	3.110	2.198	1.843	2.135	1.729	1.433		
10^{6}	12.077	11.411	6.216	4.061	7.577	4.522	3.603	3.629	3.147	2.368		
Pr=130												
10^{3}	0.719	0.462	0.422	0.424	0.438	0.405	0.407	0.443	0.408	0.410		
10^{4}	2.67	1.869	1.156	1.109	1.065	0.794	0.775	1.054	0.789	0.771		
10^{5}	6.125	5.406	3.069	2.385	3.106	2.198	1.844	2.134	1.729	1.433		
10^{6}	12.142	11.451	6.212	4.062	7.585	4.516	3.602	3.629	3.146	2.369		
	Position II ($L_{b,l}=2L/3$, $L_{b,u}=L/3$)											
					Pr=0.7							
10^{3}	0.715	0.462	0.433	0.437	0.420	0.401	0.404	0.425	0.407	0.410		
10^{4}	2.48	1.889	1.066	1.058	1.139	0.786	0.780	1.084	0.770	0.766		
10 ⁵	5.476	4.882	2.894	2.075	3.685	2.317	1.777	2.301	1.688	1.394		
10^{6}	10.925	9.968	7.053	3.524	8.287	6.017	3.275	4.020	3.394	2.312		
					Pr=10							
10^{3}	0.719	0.463	0.434	0.438	0.420	0.401	0.404	0.425	0.407	0.410		
10^{4}	2.666	1.941	1.087	1.070	1.165	0.795	0.789	1.096	0.776	0.771		
10 ⁵	6.102	5.294	3.077	2.153	4.120	2.533	1.869	2.398	1.754	1.433		
10^{6}	12.077	10.714	7.710	3.638	9.165	6.789	3.415	4.173	3.562	2.368		
			1		Pr=130				1			
10^{3}	0.719	0.463	0.434	0.438	0.420	0.401	0.404	0.425	0.407	0.410		
104	2.67	1.939	1.087	1.070	1.165	0.795	0.789	1.096	0.776	0.771		
10 ⁵	6.125	5.293	3.078	2.153	4.123	2.537	1.871	2.399	1.755	1.433		
10^{6}	12.142	10.718	7.711	3.640	9.163	6.789	3.416	4.173	3.564	2.369		

Table 2 Average Nusselt number values \overline{Nu} for cold left wall and hot right wall (buoyancy opposing boundary condition).

Position I ($L_{b,l}=L/3$, $L_{b,u}=2L/3$)												
	$H_{b,u}$	$H_u^*/3$	$2H_{u}^{*}/3$	$H_{\rm u}^*$	$H_u^*/3$	$2H_{u}^{*}/3$	$\operatorname{H}^*_{\operatorname{u}}$	$H_u^*/3$	$2H_u^*/3$	H_{u}^{*}		
Ra	No Baffle	$H_{b,l} = H_1^*/3$			$H_{b,l} = 2H_1^*/3$			$\mathbf{H}_{\mathrm{b,l}} = \mathbf{H}_{\mathrm{l}}^{*}$				
Pr=0.7												
10^{3}	0.6153	0.447	0.413	0.415	0.428	0.401	0.403	0.432	0.403	0.406		
10^{4}	1.922	1.356	0.929	0.889	0.923	0.715	0.696	0.922	0.713	0.695		
10 ⁵	4.431	3.565	2.638	1.853	2.061	1.692	1.359	1.826	1.533	1.247		
10^{6}	8.84	7.453	6.145	3.229	4.021	3.530	2.412	3.105	2.835	2.034		
Pr=10												
10^{3}	0.617	0.448	0.413	0.415	0.429	0.401	0.403	0.432	0.403	0.406		
10^{4}	1.986	1.377	0.936	0.893	0.931	0.718	0.699	0.930	0.717	0.697		
10^{5}	4.686	3.771	2.799	1.894	2.108	1.738	1.377	1.856	1.568	1.261		
10^{6}	9.358	7.880	6.540	3.302	4.205	3.708	2.470	3.154	2.899	2.058		
Pr=130												
10^{3}	0.617	0.448	0.413	0.415	0.429	0.401	0.403	0.432	0.403	0.406		
10^{4}	1.988	1.377	0.936	0.893	0.931	0.719	0.699	0.930	0.717	0.697		
10^{5}	4.694	3.774	2.800	1.895	2.108	1.738	1.377	1.856	1.568	1.261		
10^{6}	9.375	7.886	6.536	3.303	4.208	3.710	2.472	3.155	2.899	2.058		
	Position II ($L_{b,l}=2L/3$, $L_{b,u}=L/3$)											
					Pr=0.7							
10^{3}	0.6153	0.437	0.420	0.424	0.411	0.397	0.400	0.416	0.402	0.406		
10^{4}	1.922	1.265	0.880	0.873	0.933	0.700	0.697	0.923	0.697	0.695		
10^{5}	4.431	3.048	2.020	1.694	2.074	1.567	1.336	1.916	1.457	1.247		
10^{6}	8.84	6.206	3.865	2.839	3.664	3.035	2.278	3.265	2.742	2.034		
					Pr=10				_			
10^{3}	0.617	0.437	0.420	0.424	0.411	0.397	0.400	0.416	0.402	0.406		
10^{4}	1.986	1.268	0.884	0.877	0.939	0.703	0.699	0.930	0.700	0.697		
10 ⁵	4.686	3.156	2.047	1.715	2.109	1.594	1.354	1.949	1.482	1.261		
10^{6}	9.358	6.638	3.920	2.871	3.730	3.086	2.311	3.318	2.786	2.058		
2	Pr=130											
10^{3}	0.617	0.437	0.420	0.424	0.411	0.397	0.400	0.416	0.402	0.406		
104	1.988	1.266	0.883	0.876	0.939	0.703	0.699	0.930	0.700	0.697		
10 ⁵	4.694	3.154	2.044	1.714	2.107	1.594	1.354	1.949	1.482	1.261		
10^{6}	9.375	6.644	3.913	2.870	3.729	3.084	2.311	3.318	2.785	2.058		

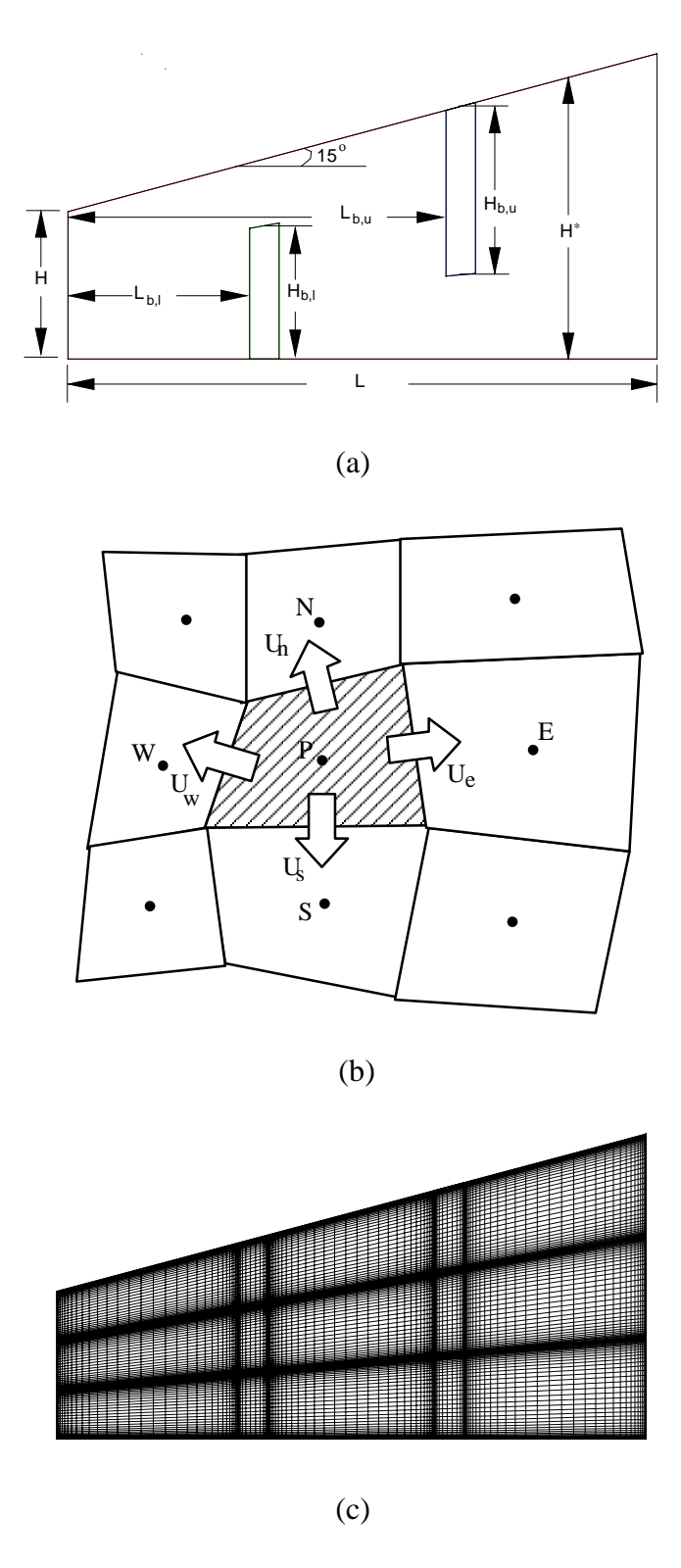


Figure 1 (a) Physical domain; (b) a typical control volume; (c) computational domain and an illustrative grid network.

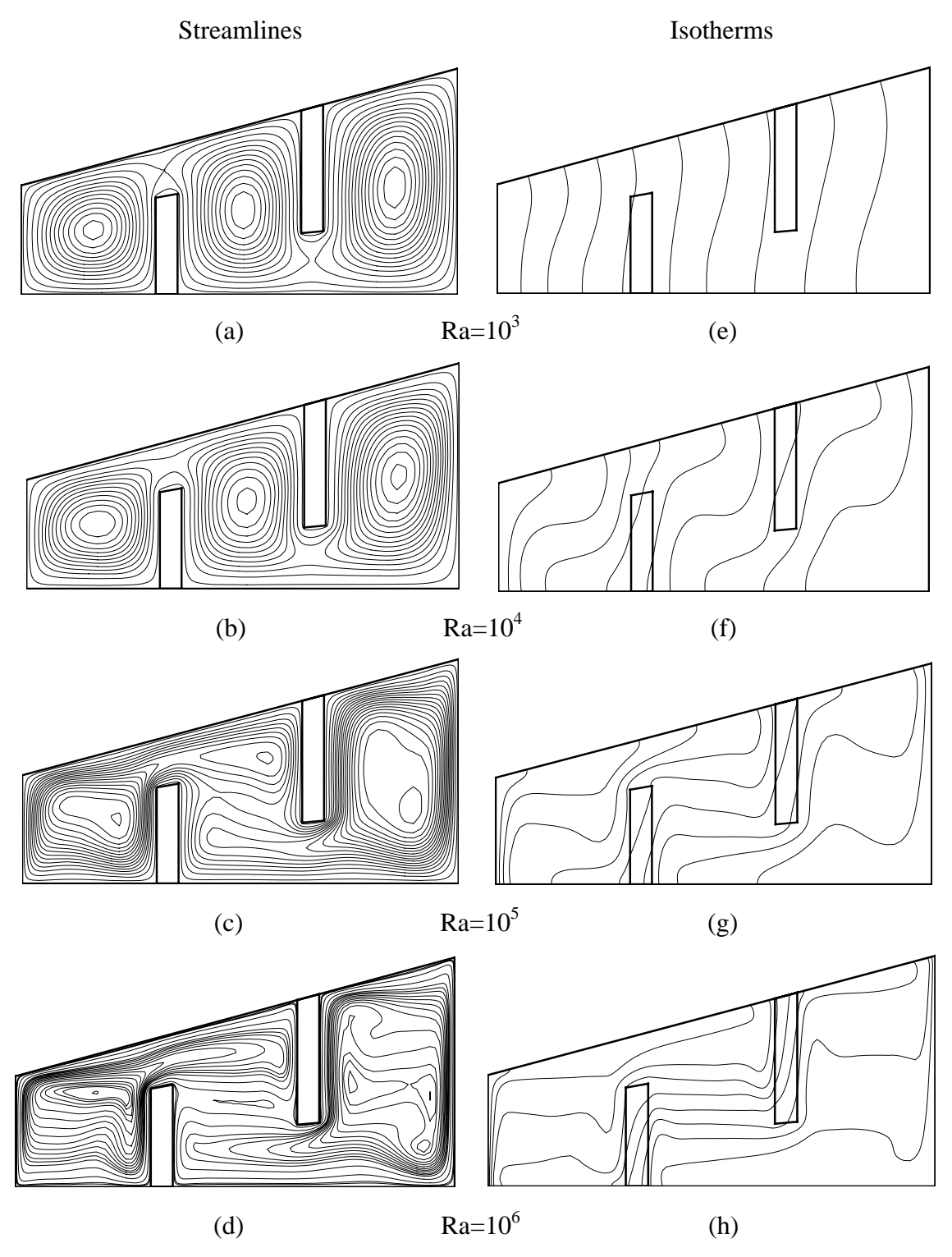


Figure 2 Streamline and isotherm plots ($H_{b,u}=2H_u^*/3$, $H_{b,l}=2H_l^*/3$, Position I) for the buoyancy assisting boundary condition.

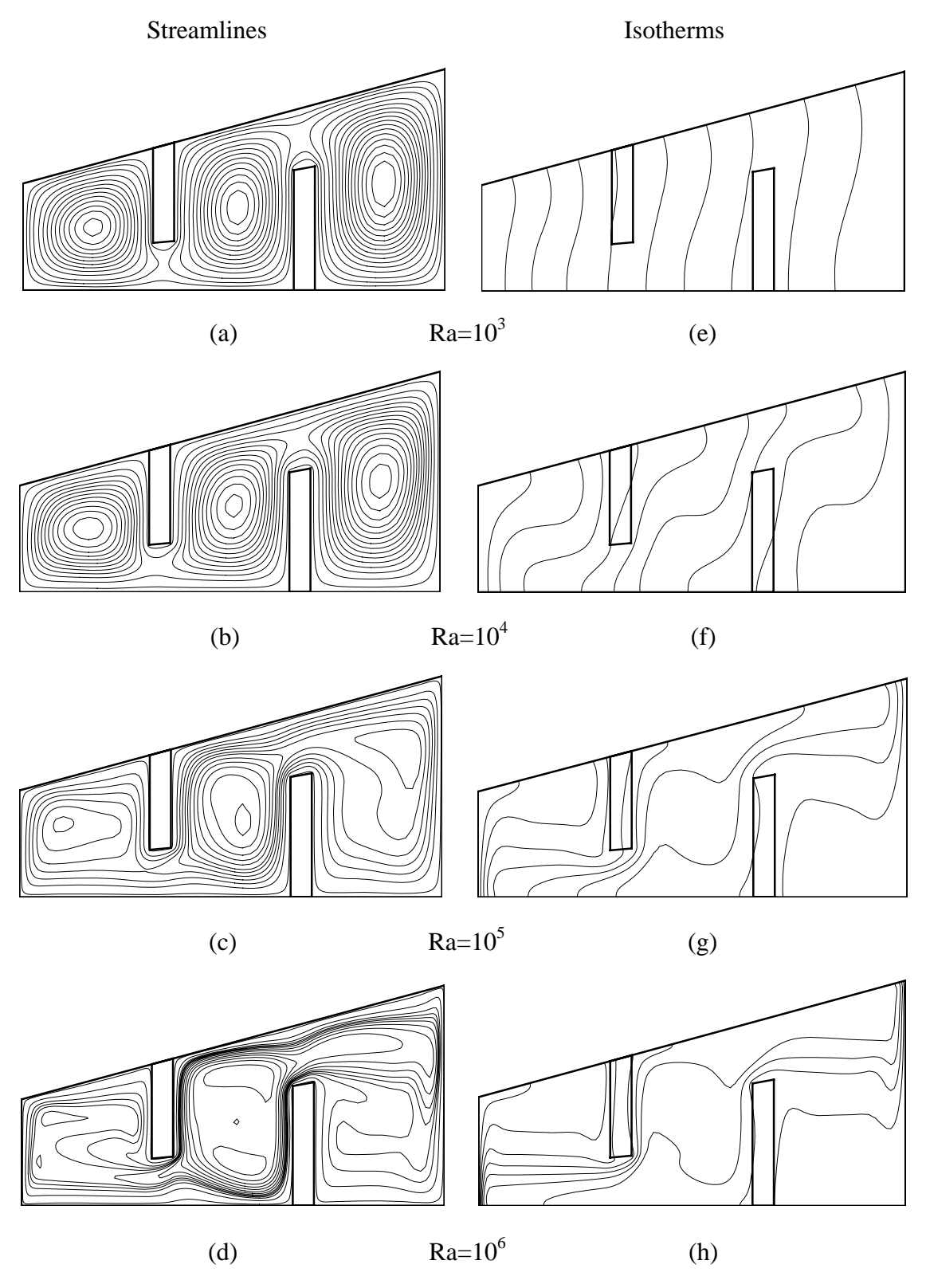


Figure 3 Streamline and isotherm plots ($H_{b,u}=2H_u^*/3$, $H_{b,l}=2H_l^*/3$, Position II) for the buoyancy assisting boundary condition.

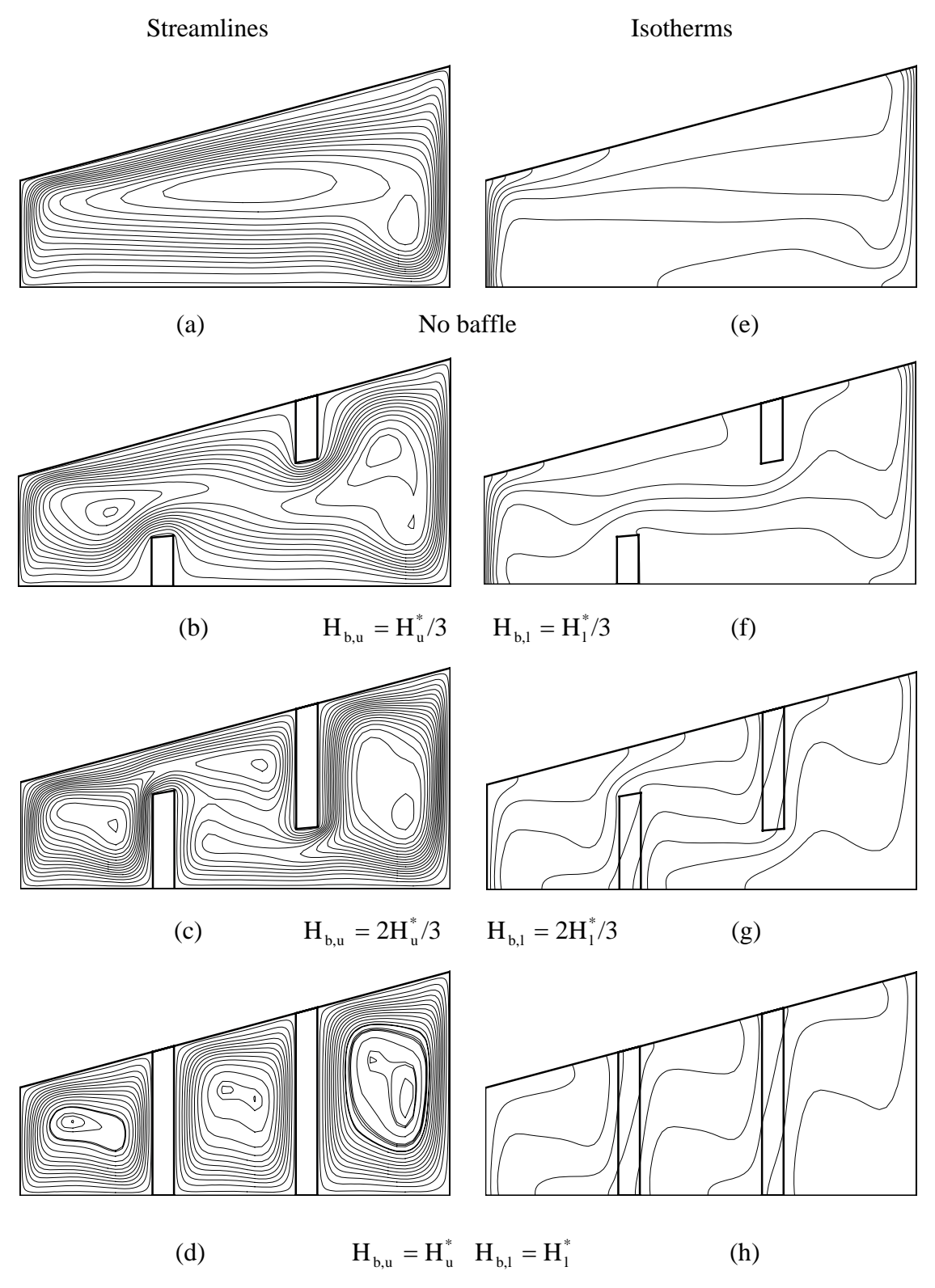


Figure 4 Streamline and isotherm plots (Ra=10⁵, Position I) at different baffles height for the buoyancy assisting boundary condition.

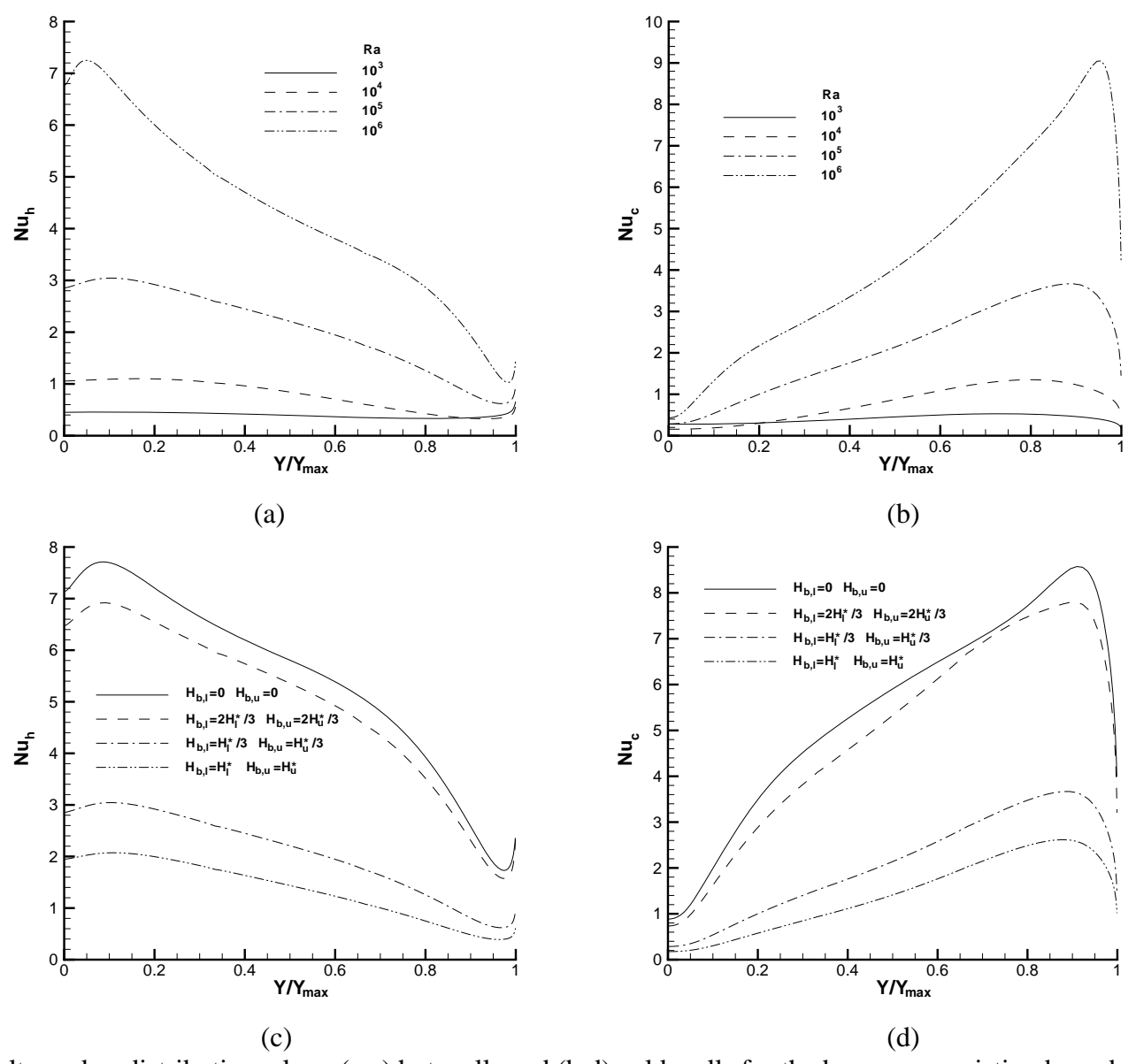


Figure 5 Local Nusselt number distribution along (a,c) hot walls and (b,d) cold walls for the buoyancy assisting boundary condition, Position I; (a,b) effects of Ra $(H_{b,u} = H_u^*/3, H_{b,l} = H_l^*/3)$; (c,d) effects of baffle heights (Ra=10⁵).

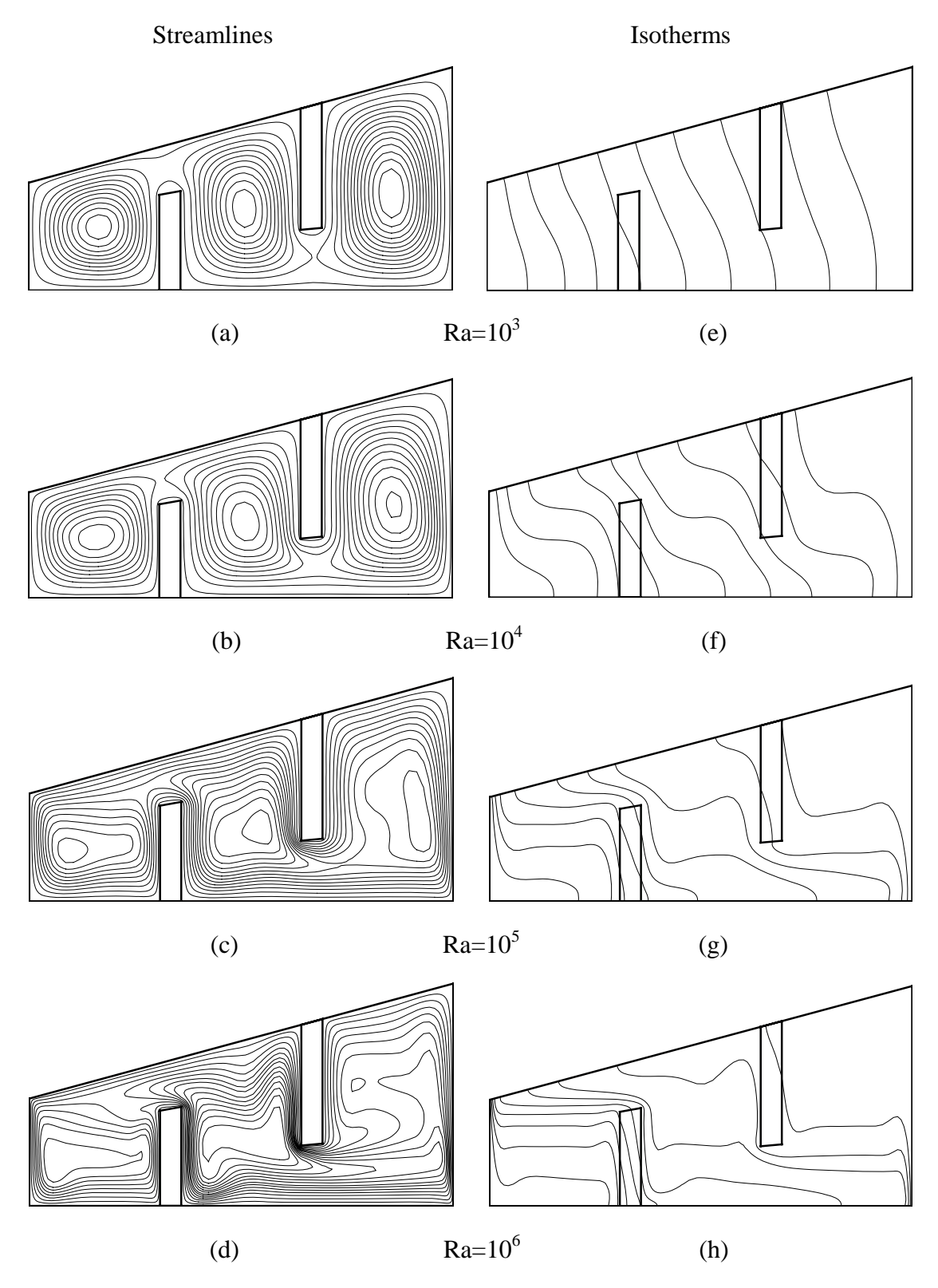


Figure 6 Streamline and isotherm plots ($H_{b,u} = 2H_u^*/3$, $H_{b,l} = 2H_l^*/3$, Position I) for the buoyancy opposing boundary condition.

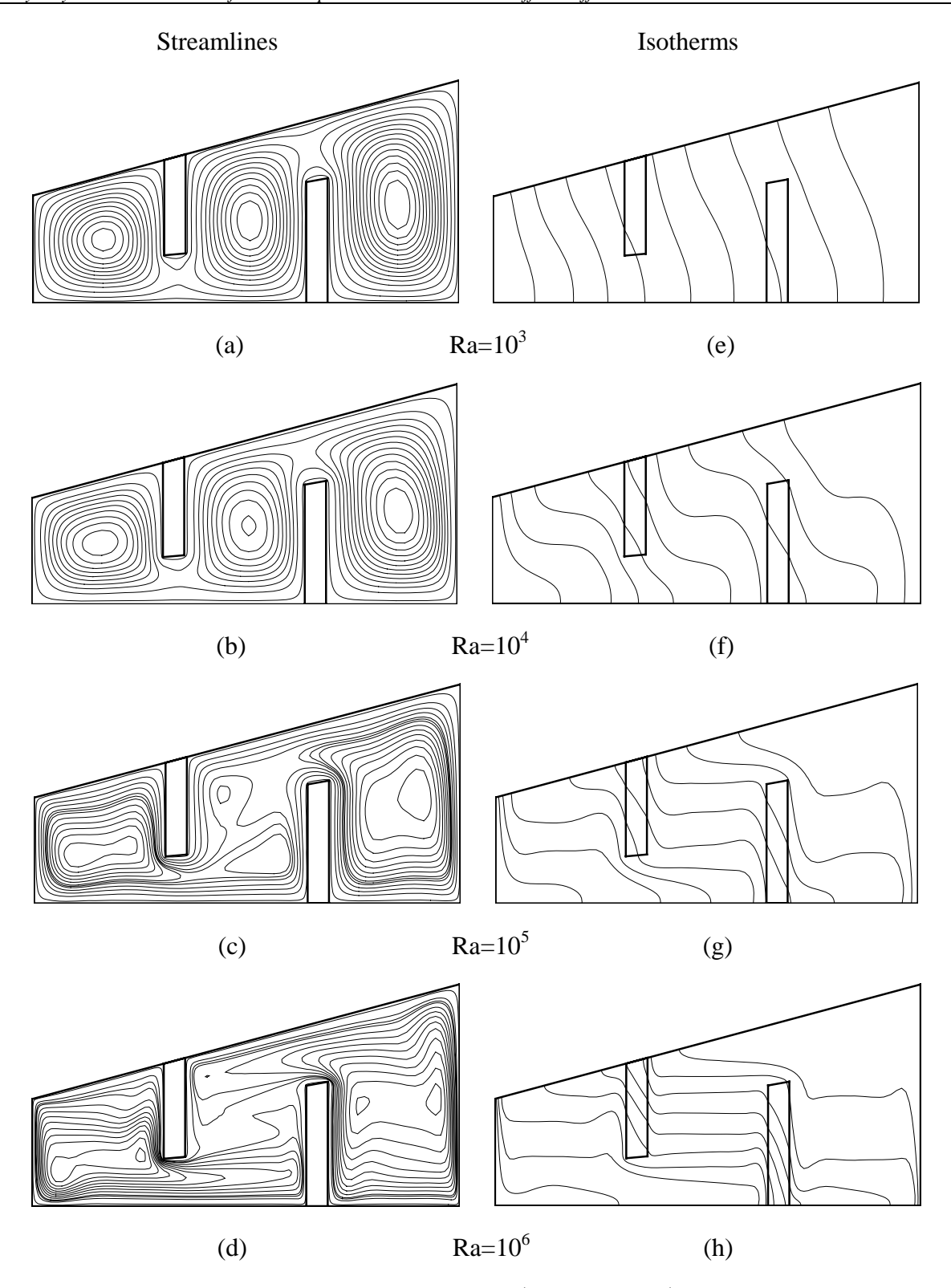


Figure 7 Streamline and isotherm plots ($H_{b,u}=2H_u^*/3$, $H_{b,l}=2H_l^*/3$, Position II) for the buoyancy opposing boundary condition.

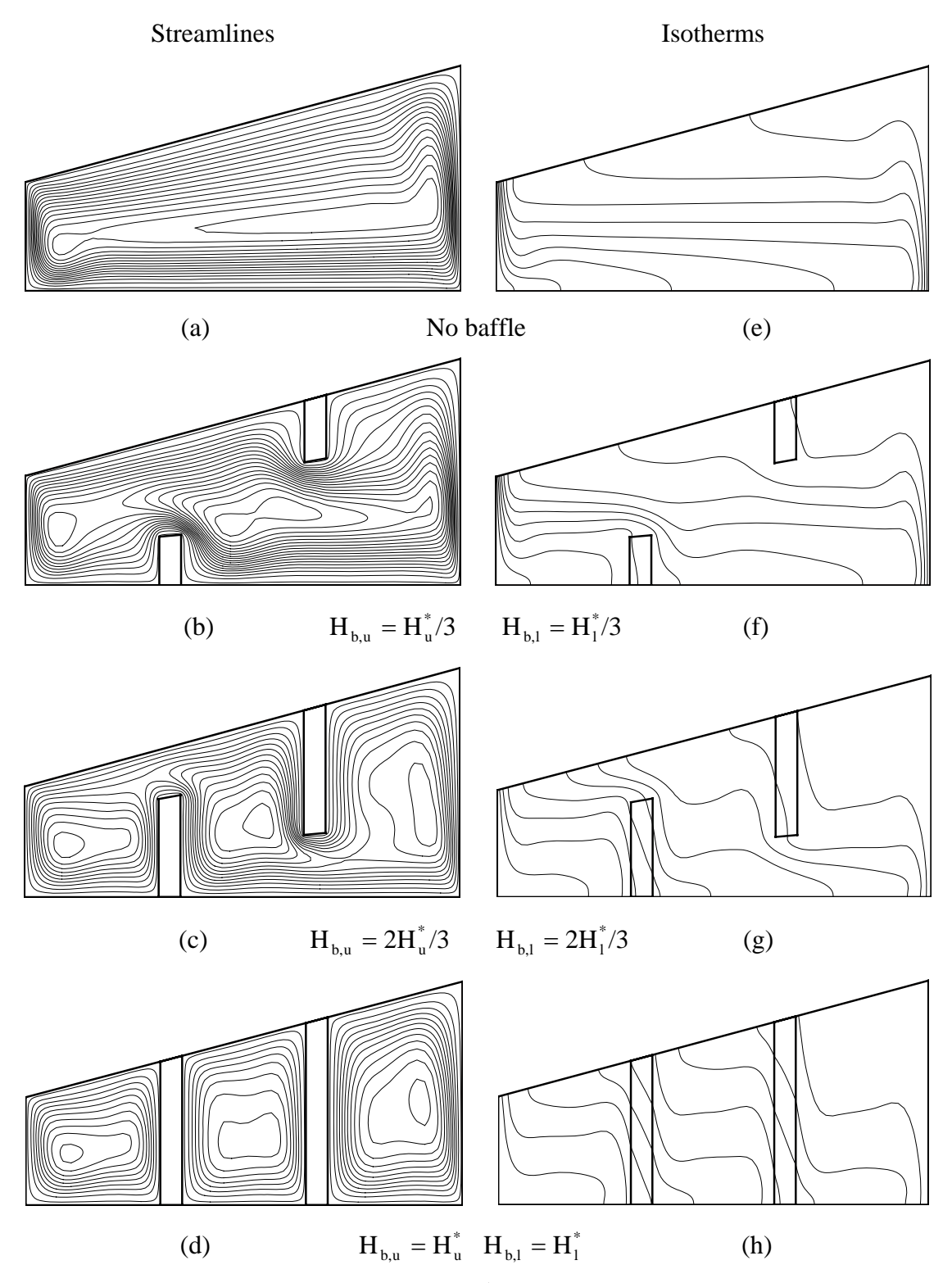


Figure 8 Streamline and isotherm plots (Ra=10⁵, Position I) at different baffles height for the buoyancy opposing boundary condition.

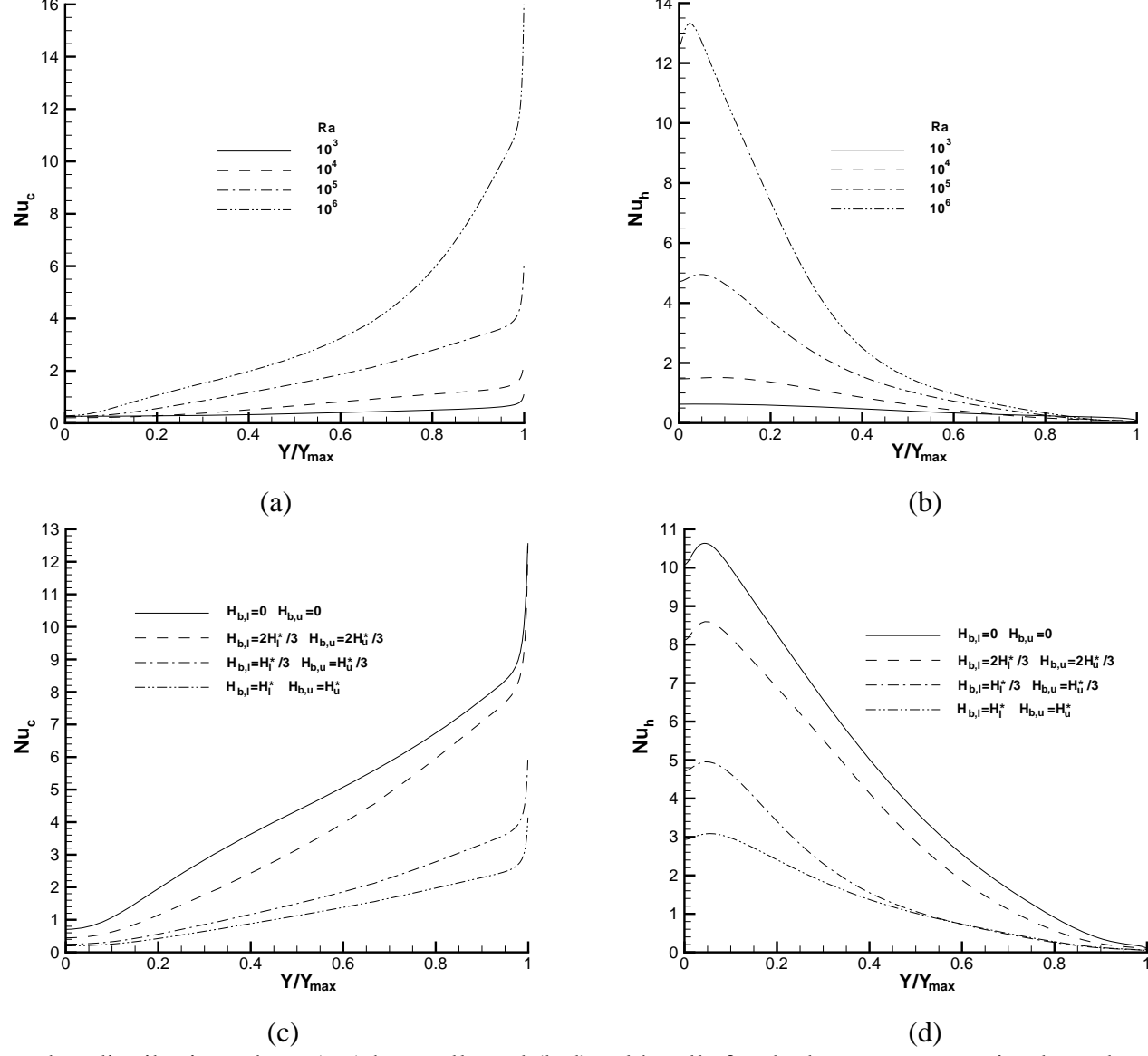


Figure 9 Local Nusselt number distribution along (a,c) hot walls and (b,d) cold walls for the buoyancy opposing boundary condition, Position I; (a,b) effects of Ra $(H_{b,u} = H_u^*/3, H_{b,l} = H_l^*/3)$; (c,d) effects of baffle heights (Ra=10⁵).